

Synergistic Multiscale Detail Refinement via Intrinsic Supervision for Underwater Image Enhancement

Dehuan Zhang^{1*}, Jingchun Zhou^{1*†}, Chunle Guo², Weishi Zhang¹, Chongyi Li²

¹ College of Information Science and Technology, Dalian Maritime University

² VCIP, CS, Nankai University

zhangdehuan97@gmail.com, zhoujingchun03@gmail.com, guochunle@nankai.edu.cn, teesiv@dlmu.edu.cn, lichongyi@nankai.edu.cn

Abstract

Visually restoring underwater scenes primarily involves mitigating interference from underwater media. Existing methods ignore the inherent scale-related characteristics in underwater scenes. Therefore, we present the synergistic multi-scale detail refinement via intrinsic supervision (SMDR-IS) for enhancing underwater scene details, which contain multi-stages. The low-degradation stage from the original images furnishes the original stage with multi-scale details, achieved through feature propagation using the Adaptive Selective Intrinsic Supervised Feature (ASISF) module. By using intrinsic supervision, the ASISF module can precisely control and guide feature transmission across multi-degradation stages, enhancing multi-scale detail refinement and minimizing the interference from irrelevant information in the low-degradation stage. In multi-degradation encoder-decoder framework of SMDR-IS, we introduce the Bifocal Intrinsic-Context Attention Module (BICA). Based on the intrinsic supervision principles, BICA efficiently exploits multi-scale scene information in images. BICA directs higher-resolution spaces by tapping into the insights of lower-resolution ones, underscoring the pivotal role of spatial contextual relationships in underwater image restoration. Throughout training, the inclusion of a multi-degradation loss function can enhance the network, allowing it to adeptly extract information across diverse scales. When benchmarked against state-of-the-art methods, SMDR-IS consistently showcases superior performance. The code is publicly available at: <https://github.com/zhoujingchun03/SMDR-IS>

Introduction

In the complex dynamics of underwater environments, the quality of optical images is primarily determined by the influence of dissolved and suspended substances on light absorption and scattering (Guo et al. 2023). Absorption effects lead to challenges like reduced imaging distance and color distortion, while scattering effects diminish image contrast and detail. Our goal is to enhance the quality of underwater optical images, providing robust solutions for applications, such as underwater exploration, marine biology research, and surveillance (Liu et al. 2022b). Image enhance-

*These authors contributed equally.

†Corresponding author

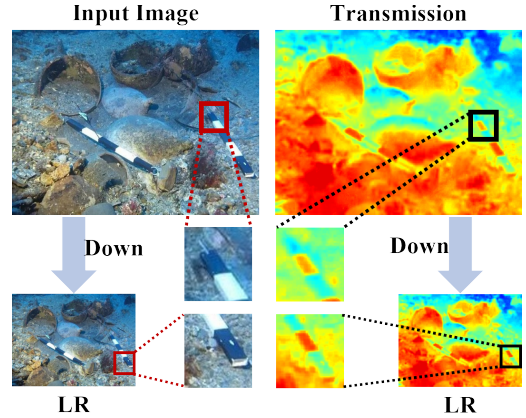


Figure 1: Illustration of motivation. The figure showcases similar scene information extracted from multi-resolution images alongside transmission. Degradation patterns, consistent across different positions, are evident in both the original and the downsampled images.

ment technique empowers researchers and practitioners to more effectively interpret and analyze underwater image data (Kang et al. 2022).

Enhancing low-quality images poses significant challenges to the field of computer vision (Ma et al. 2023; Khan et al. 2023; Zhou et al. 2024). These challenges arise primarily from scattering and blurring effects unique to aquatic environments, which inherently manifest in a multi-scale manner (Zhou et al. 2023b). Particulate matter and water turbulence at different scales have different effects on different scales have different effects on different parts of an image, leading to the degradation of multi-scale correlated features. The underwater image formation model (UIFM) (Zhou et al. 2023e) is represented as:

$$I = J \times t + A(1 - t) \quad (1)$$

where I represents the clear image, J is the underwater image, t represents the transmission related to depth, and A denotes the atmospheric light.

The core objective of underwater image enhancement (UIE) is to accurately estimate I from Eq. (1) (Zhou et al. 2023a). This is crucial because degradation levels in underwater images can differ across pixels due to variations in

distance. There are many existing enhancement techniques (Zhuang, Li, and Wu 2021), which either globally or locally extract features (Liu et al. 2022a) (Liu et al. 2023). These methods often leverage filters (Zhou et al. 2023c) and color correction techniques (Zhou et al. 2022) to improve image quality. As illustrated in Figure 1, similar degradation scenarios exist in different resolution stages. Therefore, the inherent scale-related characteristics in multi-scale underwater scenes (Jiang et al. 2020)(Hou et al. 2023) demand attention. By recognizing inherent scale-related degradation patterns, we can gain a richer understanding of the structure of the scene. In light of this, we proposed Synergistic Multi-scale Detail Refinement via Intrinsic Supervision for Underwater Image Enhancement (SMDR-IS). SMDR-IS uniquely leverages low-resolution images as auxiliary inputs, providing additional insights into scene degradation.

SMDR-IS simultaneously harnesses multiple degradations to mitigate the loss of multiple scene features resulting from feature extractions. While feature extraction at the original yields high-level features produce high-level features, it is often possible to capture finer data features at the expense of larger-scale scene information. The low-degradation stages serve to counteract the excessive abstraction from redundant extractions, ensuring that the intrinsic relationship between features and the original image remains intact. By integrating low-degradation images and features from the initial layers, both credibility and applicability are enhanced. Furthermore, the incorporation of ASISF guarantees that irrelevant information is excluded from the original resolution.

The contributions are summarized as follows:

(1) Addressing the limitations of scale-related features in current underwater image enhancement methods, which lead to incomplete restoration of scene details, we propose a synergistic multiscale detail refinement via intrinsic supervision for underwater image enhancement.

(2) We design a new attention, namely Bifocal Intrinsic-Context Attention, based on a dual-path approach, ensuring that both feature enhancement and contextual semantic information are addressed. Additionally, we integrate resolution-guided supervision to boost computational efficiency without sacrificing detail enhancement quality.

(3) With the aim of refining low-resolution feature information, we introduce the Adaptive Selective Intrinsic Supervised Feature (ASISF) module. ASISF regulates feature propagation, enhancing image quality and avoiding blurring caused by utilizing the overlay of multiscale scene details.

(4) The integration of a multi-degradation loss function provides constraints and optimization for learning features at each stage. This approach empowers the network to effectively exploit information at various scales, thereby improving detail and structure recovery.

Related Work

UIE techniques have become increasingly prevalent in the domains of computer vision and image processing (Zhuang et al. 2022). Broadly speaking, deep learning-based UIE methods can be divided into prior-based methods and end-to-end methods.

Prior-based Image Enhancement

Prior-based methods rely on explicit degradation models or pre-existing knowledge to calibrate model parameters. For instance, UColor (Li et al. 2021) which is guided by transmission, employs a transmission-driven image enhancement network using GDCP (Peng, Cao, and Cosman 2018). (Zhou et al. 2023d) uses an augmented U-Net to fuse inputs, such as the original, color-corrected, and contrast-enhanced images, to effectively leverage features. Unsupervised underwater image restoration method (USUIR) (Fu et al. 2022) involves designing a transmission subnet, a global background subnet, and a scene radiance subnet to estimate parameters of UIFM, facilitating Photo-realistic image restoration. Zhang et al. (Zhang et al. 2023) proposed Rex-Net, which applied the Retinex theory to enhance underwater images. (Mu et al. 2023) employs physical knowledge to design the Adaptive Transmission-Guided Module to guide the network. While these methods have shown promising results, the intricate and unpredictable nature of underwater environments sometimes undermines the efficacy of the proposed priors, potentially limiting model adaptability.

End-to-end Image Enhancement

End-to-end UIE techniques circumvent the need for explicit degradation models or prior knowledge. UIEC² (Wang et al. 2021) enhanced image in the RGB and HSV color spaces. UIEC² employs RGB pixel-level blocks for color restoration and adjusts saturation using curves in the HSV domain. In (Zhou, Zhang, and Zhang 2023), an enhancement method is devised based on cross-view images, which employs feature alignment to fuse scene information from multiple perspectives. Liu et al. (Jiang et al. 2022b) put forth an image-aware adversarial fusion network rooted in object detection. This strategy integrates a multi-scale dense enhancement subnet to bolster visual results. (Khan et al. 2023) proposed a lightweight transformer method (UIEPTA), which presents a gray-scale attention model to guide the network for extracting non-contaminated features. Notwithstanding their merits, many existing end-to-end methods tend to overlook the full potential of scale-related features in image scenes. This oversight often results in difficulties in precise scene detail recovery. To address this gap, we introduce SMDR-IS, emphasizing synergistic multiscale detail refinement and intrinsic supervision.

Methodology

We propose Synergistic Multiscale Detail Refinement via Intrinsic Supervision for Underwater Image Enhancement (SMDR-IS), as depicted in Figure 2. SMDR-IS comprises a multi-degradation encoder and decoder.

Multi-Degradation Encoder

Our proposed model integrates four stages of multi-resolution image inputs, equipping the network and the related features with diverse scale scene information of the input image. Initially, we employ downsampling on the original image to derive underwater scenes of different

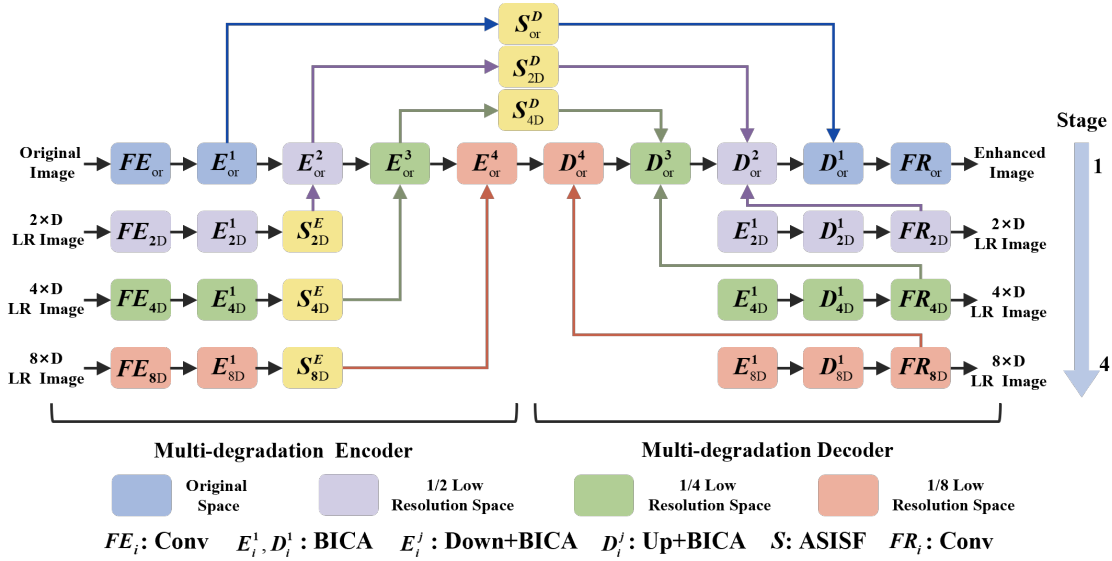


Figure 2: The overview of SMDR-IS. In Decoder, E_i^1 is the same as in Encoder. FE_i , $i \in \{or, 2D, 4D, 8D\}$ is Feature Extraction (Conv). E_i^1 , D_i^1 denote the Bifocal Intrinsic-Context Attention (BICA). E_i^j , $j \in [2, 4]$ is Downsampling+BICA. D_i^j is Upsampling+BICA. S denotes Adaptive Selective Intrinsic Supervised Feature Module (ASISF). FR_i is Feature Restoration (Conv).

scales. Since prevailing UNet-based underwater enhancement methods (Li et al. 2021) typically utilize three downsampling steps, we adopt three downscaled stages corresponding to each stage of the UNet. This can capture a richer array of scale scene information. To harness the scale-correlated attributes of image scenes, SMDR-IS proposed the multi-degradation encoder, further supplemented by three stages for lower-resolution images.

Each encoder stage incorporates the Bifocal Intrinsic-Context Attention Module (BICA) to extract feature details. BICA can adeptly fuse global and local features, optimizing image enhancement. With the aid of resolution-guided supervision, BICA strikes a harmonious balance between computational efficiency and details enhancement. To bolster the utility of low-resolution features, we proposed the Adaptive Selective Intrinsic Supervised Feature (ASISF) module. This module governs feature propagation, elevating image enhancement outcomes, and curbing information blurring that may arise from superimposing multi-scale scene details.

Bifocal Intrinsic-Context Attention The bifocal intrinsic-context attention module (BICA), as depicted in Figure 3, consists of two distinct branches. The first branch is responsible for recognizing the significant influence of neighboring pixel regions for image restoration. This branch contains the Comprehensive Feature Attention (CFA) module (detailed in the supplementary material), followed by the Resolution-Guided Intrinsic Attention (ReGIA) module. The CFA module, as shown in Figure 3 (b), extracts features from pixels and channels through spatial attention and channel attention, respectively. The features from CFA are fed to the ReGIA module, whose function is to broaden the receptive field while maintaining computational efficiency. As shown

in Figure 3(c), by using low-resolution spatial intrinsic supervision, ReGIA can further enrich the features by effectively capturing multi-scale scene details.

In the second branch, acknowledging the pivotal role of spatial contextual relationships in underwater image restoration, we design the Hierarchical Context-Aware Feature Extraction (HCAFE) module (detailed in the supplementary material). This module functions within the original feature domain, extracting image representation features through hierarchical context attention.

BCIA leverages a resolution-guided supervision approach, achieving superior computational efficiency without sacrificing detail quality. BCIA employs an innovative dual-path attention mechanism, comprehensively addressing both the influence of neighboring pixel regions and spatial contextual relationships.

Resolution-Guided Intrinsic Attention Module Underwater image optimization is heavily influenced by the contextual details of adjacent pixels. However, to reduce the computational efficiency of the network, enhancement methods often utilize compact 3×3 convolutional kernels for feature extraction. Although 3×3 kernels are computationally efficient, the small receptive field hinders the network to capture extensive contextual features.

To address the limitation and broaden the receptive field, we propose the Resolution-Guided Intrinsic Attention Module (ReGIA), which enhances the preliminary features extracted from the input image by CFA. ReGIA is tailored to discern feature weight data in a lower-resolution latent space with a large feature receptive field. Guided by the lower-resolution latent space, ReGIA serves as a guiding beacon that not only enhances the correlation of features in the orig-

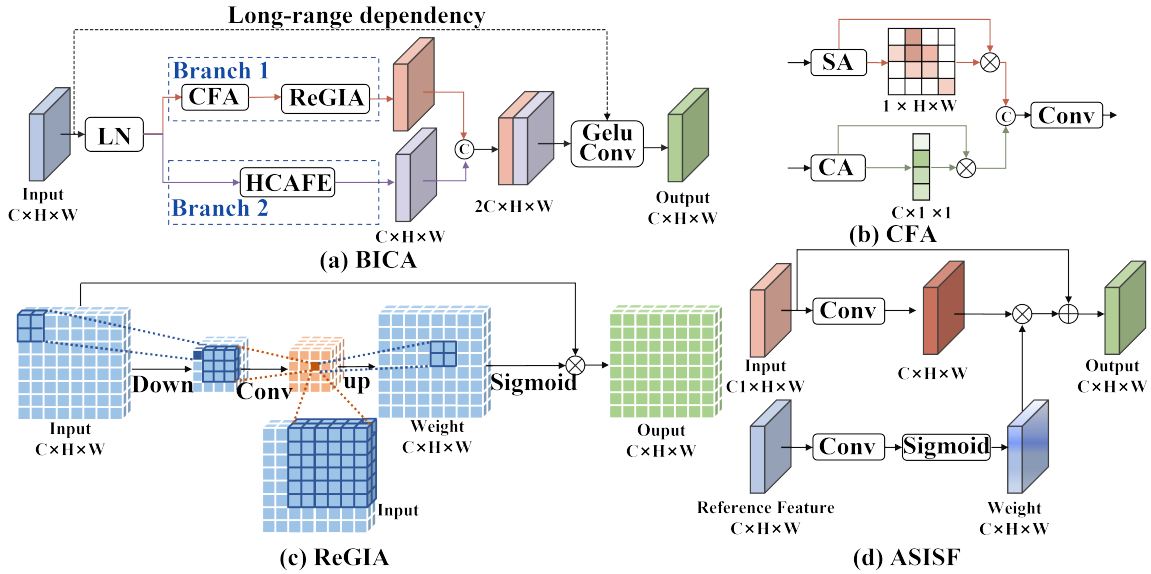


Figure 3: (a) Architecture of BICA, LN represents Layer Normalization. (b) CFA, CA and SA represent Channel Attention and Spatial Attention, respectively. (c) ReGIA, "Down" and "Up" denote downsampling and upsampling, respectively. In low-resolution, 1×1 corresponds to 6×6 spatial feature in the original resolution. (d) ASISF, highlighting that the channels in both input and reference features can be diverse.

inal domain but also strives to improve the computational efficiency of the network.

Adaptive Selective Intrinsic Supervised Feature Module When integrating feature information from the low-resolution encoder and decoder into the original resolution branch, it is imperative to mitigate interference from non-essential information during image restoration (Zamir et al. 2021). To this end, we introduce the Adaptive Selective Intrinsic Supervised Feature Module (ASISF). This module adopts an intrinsic-supervised approach for feature selection and constraint, as depicted in Figure 3.

ASISF is meticulously designed to retain only the most pertinent features to supplement image feature extraction and reconstruction in the original resolution stage. When learning features from the low-resolution encoder, the features from the original resolution act as a reference. This strategy ensures that both the encoder and decoder components of multi-degradation align with the genuine degradation traits inherent in underwater images.

This is particularly significant in the context of image restoration, where the presence of noise, distortions, and varying levels of degradation can complicate the restoration process. By employing intrinsic supervision, ASISF effectively identifies and retains features meaningful for the restoration task, thereby improving the precision and efficiency of the restoration process. The feature adaptive selection is pivotal for effective learning and generalization of the SMDR-IS, ultimately enhancing image restoration capabilities by supplementing inherent scale-related degradation patterns at multi-resolution.

Multi-Degradation Decoder

Unlike the traditional UNet, the multi-degradation decoder in SMDR-IS is uniquely designed to complement its encoder counterpart. Low-degradation information captures the inherent scale-related characteristics of input images. By integrating this information, the decoder can gain a deeper insight into these degradation patterns and multiple scenes.

The fusion of low-degradation and residual information from the encoder equips the decoder with a holistic grasp of the complicated image degradation. This comprehensive understanding empowers the network to produce restoration results that are both precise and context-rich. Essentially, the low-degradation information acts as the supplementary branch, enhancing the decoder's restoration capabilities. Consequently, the output images not only exhibit crisp details but also accurately recover information from multiple scenes. It is worth mentioning that within the FR_{iD} , the ASISF performs intrinsic-supervised feature selection on the output features when feeding data to the original degradation encoder. This ensures that only the most relevant feature is propagated through the image processing pipeline. In essence, the multi-degradation decoder of SMDR-IS uses low-degradation cues to ingeniously supplement inherent scale-related characteristics, thereby notably improving the fidelity of the restored images.

Multi-Degradation Loss Function

To enhance the precision of the restoration process, SMDR-IS employs a multi-degradation loss function to govern different modules of the network, which compares the multi-resolution enhancement image of SMDR-IS with multi-resolution ground truth, to instill multi-resolution supervi-

| | | | | | | | | | | |
|-----------|--------------|--------------|--------------|--------------|--------------|--------------|--------------|--------------|--------------|---------------------|
| | | | | | | | | | | |
| PSNR SSIM | 9.61 0.72 | 14.23 0.84 | 12.36 0.78 | 17.66 0.89 | 13.68 0.68 | 17.99 0.88 | 21.93 0.93 | 24.99 0.94 | 23.85 0.81 | 31.04 0.97 |
| | | | | | | | | | | |
| PSNR SSIM | 11.80 0.66 | 11.73 0.68 | 8.60 0.48 | 14.27 0.76 | 12.72 0.66 | 19.75 0.91 | 22.35 0.92 | 25.37 0.94 | 22.51 0.81 | 29.12 0.98 |
| | | | | | | | | | | |
| PSNR SSIM | 15.69 0.76 | 15.84 0.78 | 8.97 0.67 | 13.96 0.74 | 16.27 0.67 | 15.96 0.84 | 20.08 0.88 | 25.16 0.95 | 18.91 0.73 | 26.83 0.95 |
| | | | | | | | | | | |
| CCF CEIQ | 25.36 3.46 | 21.01 3.22 | 23.71 3.17 | 22.70 3.28 | 10.42 2.42 | 24.83 3.31 | 24.32 3.38 | 22.56 3.23 | 21.89 3.23 | 28.19 3.52 |
| | | | | | | | | | | |
| CCF CEIQ | 23.27 3.33 | 24.85 3.51 | 24.94 3.44 | 20.59 3.32 | 10.98 2.57 | 22.57 3.33 | 22.78 3.40 | 25.15 3.52 | 16.70 3.06 | 31.41 3.60 |
| | | | | | | | | | | |
| PSNR SSIM | 16.46 0.82 | 21.93 0.94 | 13.98 0.76 | 15.92 0.86 | 21.41 0.87 | 21.15 0.94 | 24.84 0.90 | 23.79 0.95 | 20.73 0.80 | 29.64 0.97 |
| | | | | | | | | | | |
| PSNR SSIM | 14.81 0.86 | 24.44 0.95 | 13.66 0.86 | 24.85 0.97 | 17.33 0.84 | 15.42 0.89 | 20.41 0.94 | 20.01 0.94 | 24.04 0.91 | 25.85 0.97 |
| | | | | | | | | | | |
| PSNR SSIM | 17.22 0.86 | 17.46 0.87 | 9.78 0.69 | 24.72 0.95 | 21.90 0.84 | 20.65 0.93 | 22.61 0.86 | 24.49 0.95 | 20.13 0.79 | 31.42 0.97 |
| Raw | ULAP | IBLA | GDPC | Waternet | FUnIEGAN | UWCNN | UColor | UDA | U-shape | SMDR-IS |

Figure 4: Qualitative comparison between state-of-the-art methods and the SMDR-IS on various datasets.

sion.

$$L_1 = \sum_{i=1}^N |y_i - \hat{y}_i| \quad (2)$$

$$L_{pre} = \|\phi(y)_i - \phi(\hat{y})_i\|_2^2 \quad (3)$$

$$L_{mse} = \frac{1}{N} \sum_{i=1}^N (y_i - \hat{y}_i)^2 \quad (4)$$

$$L_j = L_1^j + 0.2 \times L_{pre}^j + L_{mse}^j \quad (5)$$

where N is the total number of pixels in the image, y_i denotes the ground-truth pixel value, \hat{y}_i represents the predicted pixel value. ϕ is the function in VGGNet. i represents the i -th layer's feature maps in the pre-trained network. L_j represents the loss function of the j -th stage, j is an index, from 1 to 4. 4 is the number of stages in SMDR-IS.

The overall loss functions (L) for training SMDR-IS can be written as follows:

$$L = \sum_{j=1}^4 L_j \quad (6)$$

Experiments

Datasets

We trained SMDR-IS utilizing the UIEB dataset, which consists of 800 training images and 90 paired testing images. To assess the robustness of SMDR-IS, we further conducted the evaluation on various datasets, i.e. UIEB, U45, LSUI.

Implementation Details

Our method was implemented using PyTorch, with an NVIDIA Tesla V100 GPU, Intel(R) Xeon(R) Silver 4114 CPU, and 32GB RAM. For training, images were randomly cropped to a resolution of 256×256 , and we used a batch size of 44 and a learning rate of 0.0002. To ensure that SMDR-IS can generate outputs consistent with the original image size during testing, we adopted the border padding techniques.

Comparison Results

In this section, we adopted both objective assessments (UIQM, UCIQE (Jiang et al. 2022a), CCF (Wang et al. 2018), CEIQ (Fang et al. 2014), VSI (Zhang, Shen, and Li

| Dataset | Metric | ULAP | IBLA | GDCP | WaterNet | FUnIEGAN | UWCNN | UColor | UDA | U-shape | SMDR-IS |
|----------------|------------------|--------|--------|--------|----------|----------|--------|--------|---------------|---------------|---------------|
| UIEB Val | PSNR \uparrow | 15.913 | 17.988 | 13.386 | 17.349 | 17.114 | 17.985 | 20.962 | 21.484 | 20.462 | 23.710 |
| | MSE \downarrow | 0.174 | 0.143 | 0.228 | 0.144 | 0.150 | 0.134 | 0.097 | 0.096 | 0.100 | 0.075 |
| | SSIM \uparrow | 0.745 | 0.805 | 0.747 | 0.813 | 0.701 | 0.844 | 0.863 | 0.873 | 0.792 | 0.922 |
| | VSI \uparrow | 0.947 | 0.958 | 0.943 | 0.966 | 0.941 | 0.966 | 0.971 | 0.970 | 0.959 | 0.983 |
| | FSIM \uparrow | 0.915 | 0.928 | 0.901 | 0.908 | 0.891 | 0.923 | 0.931 | 0.932 | 0.892 | 0.967 |
| | FSIMc \uparrow | 0.878 | 0.899 | 0.865 | 0.899 | 0.858 | 0.903 | 0.920 | 0.918 | 0.883 | 0.957 |
| | UIQM \uparrow | 2.259 | 2.490 | 2.670 | 2.917 | 3.092 | 3.011 | 3.049 | 2.897 | 3.131 | 3.015 |
| | UCIQE \uparrow | 0.604 | 0.606 | 0.592 | 0.606 | 0.564 | 0.554 | 0.591 | 0.612 | 0.576 | 0.607 |
| | CCF \uparrow | 24.145 | 23.841 | 23.026 | 20.042 | 20.416 | 20.360 | 21.827 | 26.220 | 21.966 | 26.012 |
| | CEIQ \uparrow | 3.209 | 3.283 | 3.208 | 3.101 | 3.307 | 3.090 | 3.209 | 3.372 | 3.235 | 3.369 |
| ALL \uparrow | 49.441 | 51.656 | 46.109 | 47.455 | 47.733 | 48.502 | 53.226 | 58.374 | 52.997 | 60.466 | |
| U45 | UIQM \uparrow | 2.282 | 2.388 | 2.275 | 2.957 | 2.495 | 3.064 | 3.148 | 2.878 | 3.175 | 3.121 |
| | UCIQE \uparrow | 0.588 | 0.595 | 0.597 | 0.601 | 0.545 | 0.554 | 0.586 | 0.607 | 0.571 | 0.605 |
| | CCF \uparrow | 22.069 | 21.598 | 22.736 | 20.391 | 12.931 | 21.418 | 22.100 | 25.449 | 21.284 | 25.489 |
| | CEIQ \uparrow | 3.192 | 3.249 | 3.191 | 3.186 | 2.785 | 3.213 | 3.283 | 3.392 | 3.254 | 3.397 |
| | ALL \uparrow | 28.131 | 27.830 | 28.799 | 27.135 | 18.757 | 28.248 | 29.117 | 32.326 | 28.285 | 32.612 |
| LSUI | PSNR \uparrow | 17.677 | 17.555 | 13.284 | 19.990 | 21.129 | 20.368 | 21.786 | 20.288 | 20.491 | 21.984 |
| | MSE \downarrow | 0.142 | 0.149 | 0.229 | 0.109 | 0.101 | 0.102 | 0.087 | 0.104 | 0.102 | 0.089 |
| | SSIM \uparrow | 0.760 | 0.784 | 0.710 | 0.839 | 0.778 | 0.851 | 0.848 | 0.842 | 0.775 | 0.870 |
| | VSI \uparrow | 0.959 | 0.957 | 0.935 | 0.971 | 0.962 | 0.970 | 0.973 | 0.968 | 0.960 | 0.975 |
| | FSIM \uparrow | 0.925 | 0.925 | 0.886 | 0.931 | 0.920 | 0.940 | 0.940 | 0.931 | 0.900 | 0.948 |
| | FSIMc \uparrow | 0.894 | 0.894 | 0.850 | 0.918 | 0.900 | 0.921 | 0.928 | 0.912 | 0.888 | 0.933 |
| | UIQM \uparrow | 2.324 | 2.567 | 2.572 | 2.865 | 2.895 | 2.976 | 2.984 | 2.833 | 3.038 | 2.917 |
| | UCIQE \uparrow | 0.611 | 0.616 | 0.610 | 0.605 | 0.585 | 0.561 | 0.593 | 0.617 | 0.576 | 0.602 |
| | CCF \uparrow | 24.004 | 24.135 | 24.304 | 20.531 | 21.484 | 21.254 | 22.331 | 25.942 | 21.849 | 24.727 |
| | CEIQ \uparrow | 3.160 | 3.282 | 3.227 | 3.123 | 3.195 | 3.147 | 3.259 | 3.361 | 3.246 | 3.323 |
| ALL \uparrow | 51.457 | 51.864 | 47.606 | 50.882 | 52.949 | 52.091 | 54.729 | 56.799 | 52.826 | 57.368 | |

Table 1: Quantitative comparison between state-of-the-art methods and SMDR-IS on different testing datasets.

2014), PSNR (Korhonen and You 2012), MSE, SSIM (Wang et al. 2004), FSIM, FSIMc (Zhang et al. 2011)) and subjective evaluations for comprehensive analysis.

We conducted experiments to compare SMDR-IS with state-of-the-art methods to underscore its effectiveness. This includes traditional methods, such as ULAP (Song et al. 2018), IBLA (Peng and Cosman 2017), GDCP (Peng, Cao, and Cosman 2018), as well as deep learning methods, such as WaterNet (Li et al. 2019), FUnIEGAN (Islam, Xia, and Sattar 2020), UWCNN (Li, Anwar, and Porikli 2020), UColor (Li et al. 2021), UDA (Shen et al. 2023) and U-shape (Peng, Zhu, and Bian 2023). The visual results are illustrated in Figure 4, and the metrics are shown in Table 1.

To avoid any influence of color on the metrics (e.g., the impact observed with ULAP in Figure 4), we excluded the color component from CCF. As shown in Figure 4, SMDR-IS performs better than other methods in terms of visual results and performance metrics. Although ULAP, IBLA, and GDCP achieve commendable restoration results, their generalization capabilities are hindered by their dependence on priors. WaterNet and UColor display enhanced robustness but remain susceptible to extraneous inputs. Although FUnIE-GAN and UWCNN can achieve real-time efficiency, their expressive capability is somewhat constrained due to limited parameters. Although UDA and U-shape can both achieve the goal of underwater image enhancement, SMDR-IS combines the inherent scale-related features from multiple scales, providing better robustness for diverse underwa-

ter scenarios.

Table 1 tabulates the performance of different methods on the three datasets, in terms of different performance metrics. In addition to the individual performance metrics, we also combine them to form a comprehensive metric, denoted as "ALL", which is the net sum of the \uparrow values minus the \downarrow values. This measurement can provide a holistic assessment by weighing multiple criteria. Remarkably, SMDR-IS achieves the best performance, in terms of the ALL score. Collectively, these results show the ability of SMDR-IS to adeptly restore intricate scenes, underpinned by the synergy from multiscale detail extraction and intrinsic supervision.

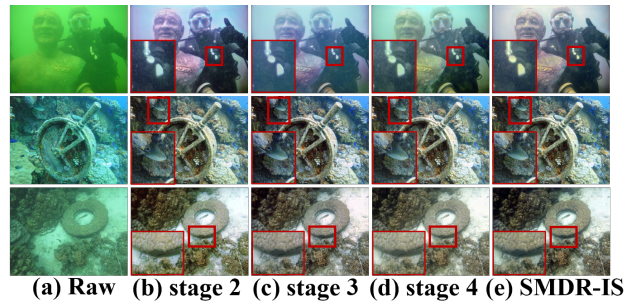


Figure 5: Subjective results of ablation experiments on number of stages used. From left to right: (a) original images, (b)-(e) correspond to lines 1-4 in Table 4.

| | ULAP | IBLA | GDCP | WaterNet | FUnIEGAN | UWCNN | UColor | UDA | U-shape | SMDR-IS |
|-----------|--------|--------|--------|----------|--------------|--------|--------|--------|---------|---------------|
| Time ↓ | 0.358 | 9.134 | 0.163 | 0.091 | 0.003 | 0.050 | 0.577 | 0.100 | 0.109 | 0.061 |
| Quality ↑ | 49.441 | 51.656 | 46.109 | 47.455 | 47.733 | 48.502 | 53.226 | 58.374 | 52.997 | 60.466 |
| Agg ↑ | 49.083 | 42.522 | 45.946 | 47.364 | 47.730 | 48.452 | 52.649 | 58.273 | 52.887 | 60.405 |

Table 2: Aggregative evaluation of efficiency and image quality.

| En | En_to.DE | De | PSNR ↑ | SSIM ↑ | ALL ↑ |
|----|----------|----|---------------|--------------|---------------|
| | ✓ | ✓ | 23.021 | 0.915 | 23.936 |
| ✓ | | ✓ | 23.697 | 0.919 | 24.615 |
| ✓ | ✓ | | 23.122 | 0.914 | 24.036 |
| ✓ | ✓ | ✓ | 23.710 | 0.922 | 24.631 |

Table 3: Ablation study for ASISF.

| S1 | S2 | S3 | S4 | PSNR ↑ | SSIM ↑ | ALL ↑ |
|----|----|----|----|---------------|--------------|---------------|
| ✓ | | | | 22.790 | 0.916 | 23.706 |
| ✓ | ✓ | | | 22.872 | 0.915 | 23.787 |
| ✓ | ✓ | ✓ | | 23.248 | 0.915 | 24.163 |
| ✓ | ✓ | ✓ | ✓ | 23.710 | 0.922 | 24.631 |

Table 4: Ablation study for the four different stages. S represents the stage.

| CA | SA | ReGIA | HCAFE | PSNR ↑ | SSIM ↑ | ALL ↑ |
|----|----|-------|-------|---------------|--------------|---------------|
| | ✓ | ✓ | ✓ | 21.219 | 0.901 | 22.120 |
| ✓ | | ✓ | ✓ | 23.352 | 0.917 | 24.269 |
| ✓ | ✓ | | ✓ | 22.673 | 0.907 | 23.580 |
| ✓ | ✓ | ✓ | | 23.276 | 0.911 | 24.186 |
| ✓ | ✓ | ✓ | ✓ | 23.710 | 0.922 | 24.631 |

Table 5: Ablation study for BICA.

| L_1 | L_{pre} | L_{mse} | PSNR ↑ | SSIM ↑ | ALL ↑ |
|-------|-----------|-----------|---------------|--------------|---------------|
| | ✓ | ✓ | 23.257 | 0.915 | 24.172 |
| ✓ | | ✓ | 22.905 | 0.912 | 23.817 |
| ✓ | ✓ | | 23.151 | 0.919 | 24.069 |
| ✓ | ✓ | ✓ | 23.710 | 0.922 | 24.631 |

Table 6: Ablation study for loss function.

Efficiency Evaluation

Table 2 presents the comprehensive analysis of efficiency, performance (the Quality is the "ALL" on UIEB Val in Table 1), and Aggregative (Agg) score. Although SMDR-IS does not obtain the highest efficiency, it still achieves a commendable frame rate of 16.4744, satisfying real-time demands. Moreover, we introduce the 'Agg' score to provide a holistic performance evaluation, which considers both efficiency and performance, specifically, $Agg = Quality \cdot Time$. As observed from Table 2, SMDR-IS achieves the highest score in Agg, which demonstrates the suitability of SMDR-IS for advanced underwater vision tasks.

Ablation Study

We performed a series of ablation experiments using the testing set from the UIEB dataset. The effects of degrada-

tion at various stages are presented in Table 4. Furthermore, we conducted ablation studies on the individual components within BICA, as detailed in 5, on the ASISF component within SMDI-IR, as illustrated in Table 3, and on the different loss functions, as showcased in Table 6. In all tables, entries in bold represent the highest scores obtained. From Table 3, it is evident that the intrinsic guidance provided by ASISF plays a pivotal role in filtering out irrelevant features during the image enhancement process.

As illustrated in Table 4 and Figure 5, the number of stages has a significant impact on the performance metrics. When increasing the number of stages, the image restoration performance and the multi-scale feature extraction capability of SMDI-IR progressively improve. The performance metrics reach the peak when the number of stages is four. It is worth noting that our choice of four stages is informed by prevalent practices, especially three-fold downsampling is commonly utilized, as highlighted in (Li et al. 2021).

The advantages of the BICA architecture are manifestly demonstrated in Table 5, where the ablation experiments highlight the image restoration ability of each module within BICA. Notably, the contribution of the proposed ReGIA to SMDI-IR is particularly significant, reaffirming the superior capabilities of ReGIA. Furthermore, to ascertain the efficacy of the loss functions used in our study, we conducted ablation experiments by sequentially omitting L_1 , L_{pre} , and L_{mse} in Table 6. These experiments collectively substantiate the effectiveness of our chosen loss functions.

Conclusion

In this study, we propose a novel method for underwater image restoration, namely SMDR-IS, which can proficiently capture multi-scale scene information, by multi-resolution detail extraction with intrinsic supervision, and utilizing the inherent scale-related features in image scenes. To ensure optimal assimilation of information across different scales, we integrated low-resolution inputs by adaptive selective intrinsic supervision within the original-resolution input, thereby amplifying the conveyance of scene information. To mitigate unnecessary interference from irrelevant scenes, we introduced ASISF, which is meticulously designed to regulate the feature propagation process. Furthermore, our multi-degradation loss function strategically guides the network during training. Optimization and constraints at each stage enhance the network's ability to leverage information at different scales. In the future, we will explore the integration of SMDR-IS into broader computer vision applications, like underwater robotics and autonomous underwater vehicles.

Acknowledgments

This work was supported in part by the Natural Science Foundation of China (Nos. 62301105), National Key Research and Development Program of China (No.2018AAA0100400), China Postdoctoral Science Foundation (NO.2021M701780), and the Cultivation Program for the Excellent Doctoral Dissertation of Dalian Maritime University. We are also sponsored by CAAI-Huawei MindSpore Open Fund and the High Performance Computing Center of Dalian Maritime University.

References

- Fang, Y.; Ma, K.; Wang, Z.; Lin, W.; Fang, Z.; and Zhai, G. 2014. No-reference quality assessment of contrast-distorted images based on natural scene statistics. *IEEE Signal Processing Letters*, 22(7): 838–842.
- Fu, Z.; Lin, H.; Yang, Y.; Chai, S.; Sun, L.; Huang, Y.; and Ding, X. 2022. Unsupervised Underwater Image Restoration: From a Homology Perspective. In *AAAI*, volume 36, 643–651.
- Guo, C.; Wu, R.; Jin, X.; Han, L.; Zhang, W.; Chai, Z.; and Li, C. 2023. Underwater Ranker: Learn Which is Better and How to Be Better. In *AAAI*, volume 37, 702–709.
- Hou, G.; Li, N.; Zhuang, P.; Li, K.; Sun, H.; and Li, C. 2023. Non-uniform Illumination Underwater Image Restoration via Illumination Channel Sparsity Prior. *IEEE Transactions on Circuits and Systems for Video Technology*.
- Islam, M. J.; Xia, Y.; and Sattar, J. 2020. Fast Underwater Image Enhancement for Improved Visual Perception. *IEEE Robotics and Automation Letters*, 5(2): 3227–3234.
- Jiang, K.; Wang, Z.; Yi, P.; Chen, C.; Huang, B.; Luo, Y.; Ma, J.; and Jiang, J. 2020. Multi-scale Progressive Fusion Network for Single Image Deraining. In *CVPR*, 8346–8355.
- Jiang, Q.; Gu, Y.; Li, C.; Cong, R.; and Shao, F. 2022a. Underwater Image Enhancement Quality Evaluation: Benchmark Dataset and Objective Metric. *IEEE Transactions on Circuits and Systems for Video Technology*, 32(9): 5959–5974.
- Jiang, Z.; Li, Z.; Yang, S.; Fan, X.; and Liu, R. 2022b. Target Oriented Perceptual Adversarial Fusion Network for Underwater Image Enhancement. *IEEE Transactions on Circuits and Systems for Video Technology*, 32(10): 6584–6598.
- Kang, Y.; Jiang, Q.; Li, C.; Ren, W.; Liu, H.; and Wang, P. 2022. A Perception-aware Decomposition and Fusion Framework for Underwater Image Enhancement. *IEEE Transactions on Circuits and Systems for Video Technology*, 33(3): 988–1002.
- Khan, M. R.; Kulkarni, A.; Phutke, S. S.; and Murala, S. 2023. Underwater Image Enhancement with Phase Transfer and Attention. In *2023 International Joint Conference on Neural Networks (IJCNN)*, 1–8. IEEE.
- Korhonen, J.; and You, J. 2012. Peak Signal-to-noise Ratio Revisited: Is Simple Beautiful? In *QoMEx*, 37–38. IEEE.
- Li, C.; Anwar, S.; Hou, J.; Cong, R.; Guo, C.; and Ren, W. 2021. Underwater Image Enhancement via Medium Transmission-guided Multi-color Space Embedding. *IEEE Transactions on Image Processing*, 30: 4985–5000.
- Li, C.; Anwar, S.; and Porikli, F. 2020. Underwater Scene Prior Inspired Deep Underwater Image and Video Enhancement. *Pattern Recognition*, 98: 107038.
- Li, C.; Guo, C.; Ren, W.; Cong, R.; Hou, J.; Kwong, S.; and Tao, D. 2019. An Underwater Image Enhancement Benchmark Dataset and Beyond. *IEEE Transactions on Image Processing*, 29: 4376–4389.
- Liu, J.; Shang, J.; Liu, R.; and Fan, X. 2022a. Attention-guided Global-local Adversarial Learning for Detail-preserving Multi-exposure Image Fusion. *IEEE Transactions on Circuits and Systems for Video Technology*, 32(8): 5026–5040.
- Liu, J.; Wu, G.; Luan, J.; Jiang, Z.; Liu, R.; and Fan, X. 2023. HoLoCo: Holistic and Local Contrastive Learning Network for Multi-exposure Image Fusion. *Information Fusion*, 95: 237–249.
- Liu, R.; Jiang, Z.; Yang, S.; and Fan, X. 2022b. Twin Adversarial Contrastive Learning for Underwater Image Enhancement and Beyond. *IEEE Transactions on Image Processing*, 31: 4922–4936.
- Ma, L.; Jin, D.; An, N.; Liu, J.; Fan, X.; Luo, Z.; and Liu, R. 2023. Bilevel fast scene adaptation for low-light image enhancement. *International Journal of Computer Vision*, 1–19.
- Mu, P.; Fang, J.; Qian, H.; and Bai, C. 2023. Transmission and Color-guided Network for Underwater Image Enhancement. In *2023 IEEE International Conference on Multimedia and Expo (ICME)*, 1337–1342. IEEE.
- Peng, L.; Zhu, C.; and Bian, L. 2023. U-shape transformer for underwater image enhancement. *IEEE Transactions on Image Processing*.
- Peng, Y.-T.; Cao, K.; and Cosman, P. C. 2018. Generalization of the Dark Channel Prior for Single Image Restoration. *IEEE Transactions on Image Processing*, 27(6): 2856–2868.
- Peng, Y.-T.; and Cosman, P. C. 2017. Underwater Image Restoration Based on Image Blurriness and Light Absorption. *IEEE transactions on image processing*, 26(4): 1579–1594.
- Shen, Z.; Xu, H.; Luo, T.; Song, Y.; and He, Z. 2023. UDAformer: Underwater image enhancement based on dual attention transformer. *Computers & Graphics*, 111: 77–88.
- Song, W.; Wang, Y.; Huang, D.; and Tjondronegoro, D. 2018. A Rapid Scene Depth Estimation Model based on Underwater Light Attenuation Prior for Underwater Image Restoration. In *Pacific Rim Conference on Multimedia*, 678–688. Springer.
- Wang, Y.; Guo, J.; Gao, H.; and Yue, H. 2021. UIEC²-Net: CNN-based Underwater Image Enhancement using Two Color Space. *Signal Processing: Image Communication*, 96: 116250.

- Wang, Y.; Li, N.; Li, Z.; Gu, Z.; Zheng, H.; Zheng, B.; and Sun, M. 2018. An Imaging-inspired No-reference Underwater Color Image Quality Assessment Metric. *Computers & Electrical Engineering*, 70: 904–913.
- Wang, Z.; Bovik, A. C.; Sheikh, H. R.; and Simoncelli, E. P. 2004. Image Quality Assessment: From Error Visibility to Structural Similarity. *IEEE Transactions on Image Processing*, 13(4): 600–612.
- Zamir, S. W.; Arora, A.; Khan, S.; Hayat, M.; Khan, F. S.; Yang, M.-H.; and Shao, L. 2021. Multi-stage Progressive Image Restoration. In *CVPR*, 14821–14831.
- Zhang, D.; Zhou, J.; Zhang, W.; Lin, Z.; Yao, J.; Polat, K.; Alenezi, F.; and Alhudhaif, A. 2023. ReX-Net: A Reflectance-guided Underwater Image Enhancement Network for Extreme Scenarios. *Expert Systems with Applications*, 120842.
- Zhang, L.; Shen, Y.; and Li, H. 2014. VSI: A Visual Saliency-induced Index for Perceptual Image Quality Assessment. *IEEE Transactions on Image processing*, 23(10): 4270–4281.
- Zhang, L.; Zhang, L.; Mou, X.; and Zhang, D. 2011. FSIM: A Feature Similarity Index for Image Quality Assessment. *IEEE Transactions on Image Processing*, 20(8): 2378–2386.
- Zhou, J.; Gai, Q.; Zhang, D.; Lam, K.-M.; Zhang, W.; and Fu, X. 2024. IACC: Cross-Illumination Awareness and Color Correction for Underwater Images Under Mixed Natural and Artificial Lighting. *IEEE Transactions on Geoscience and Remote Sensing*, 62: 1–15.
- Zhou, J.; Li, B.; Zhang, D.; Yuan, J.; Zhang, W.; Cai, Z.; and Shi, J. 2023a. UGIF-Net: An Efficient Fully Guided Information Flow Network for Underwater Image Enhancement. *IEEE Transactions on Geoscience and Remote Sensing*.
- Zhou, J.; Liu, Q.; Jiang, Q.; Ren, W.; Lam, K.-M.; and Zhang, W. 2023b. Underwater camera: Improving visual perception via adaptive dark pixel prior and color correction. *International Journal of Computer Vision*, 1–19.
- Zhou, J.; Pang, L.; Zhang, D.; and Zhang, W. 2023c. Underwater Image Enhancement Method via Multi-interval Subhistogram Perspective Equalization. *IEEE Journal of Oceanic Engineering*.
- Zhou, J.; Sun, J.; Zhang, W.; and Lin, Z. 2023d. Multi-view Underwater Image Enhancement Method via Embedded Fusion Mechanism. *Engineering Applications of Artificial Intelligence*, 121: 105946.
- Zhou, J.; Wang, Y.; Li, C.; and Zhang, W. 2023e. Multicolor Light Attenuation Modeling for Underwater Image Restoration. *IEEE Journal of Oceanic Engineering*, 48(4): 1322–1337.
- Zhou, J.; Zhang, D.; Ren, W.; and Zhang, W. 2022. Auto Color Correction of Underwater Images Utilizing Depth Information. *IEEE Geoscience and Remote Sensing Letters*, 19: 1–5.
- Zhou, J.; Zhang, D.; and Zhang, W. 2023. Cross-view Enhancement Network for Underwater Images. *Engineering Applications of Artificial Intelligence*, 121: 105952.
- Zhuang, P.; Li, C.; and Wu, J. 2021. Bayesian Retinex Underwater Image Enhancement. *Engineering Applications of Artificial Intelligence*, 101: 104171.
- Zhuang, P.; Wu, J.; Porikli, F.; and Li, C. 2022. Underwater Image Enhancement with Hyper-laplacian Reflectance Priors. *IEEE Transactions on Image Processing*, 31: 5442–5455.